RSC Advances

PAPER

View Article Online
View Journal | View Issue

Cite this: *RSC Adv.*, 2018, **8**, 16527

Shape-dependent adjuvanticity of nanoparticle-conjugated RNA adjuvants for intranasal inactivated influenza vaccines†

Taiyu Tazaki,[a] Koshiro Tabata,[b] Akira Ainai,[b] Yuki Ohara,[b] Shintaro Kobayashi,[c] Takafumi Ninomiya,[d] Yasuko Orba,[c] Hideyuki Mitomo,[ef] Tetsuo Nakano,[gh] Hideki Hasegawa,[b] Kuniharu Ijiro,[ef] Hirofumi Sawa,[ci] Tadaki Suzuki*[b] and Kenichi Niikura*[j]

Intranasal inactivated influenza vaccines can elicit mucosal immune responses that protect against virus infection. For the development of intranasal inactivated influenza vaccines, effective adjuvants inducing minimal adverse reactions are required. Generally, however, lower toxicity adjuvants have lower adjuvanticity. In this research, we fabricated nanoparticle-based adjuvants to enhance its adjuvanticity. Herein, we focused on low-molecular-weight polyinosinic-polycytidylic acid, referred to as uPIC(40:400), as a weak and less toxic RNA adjuvant. We conjugated uPIC(40:400) with different shaped gold nanoparticles (AuNPs) electrostatically. Conjugation with gold nanorods, but not spherical AuNPs, markedly enhanced the adjuvanticity of uPIC(40:400), leading to the suppression of viral infection in mice. Notably, conjugation with gold nanorods did not increase the inflammatory cytokine production in dendritic cells. These data indicated that gold nanorods can provide a good platform for enhancing the weak adjuvanticity of uPIC(40:400) while maintaining low inflammatory cytokine production toward the development of intranasal inactivated influenza vaccines.

Received 26th February 2018
Accepted 25th April 2018

DOI: 10.1039/c8ra01690a

rsc.li/rsc-advances

1. Introduction

Currently, most vaccines are applied subcutaneously (SC) or intramuscularly (IM) and the preference for the administration route can vary depending on the infectious diseases. The current standard influenza vaccine is a SC or IM injection type. Intranasal influenza vaccination has various advantages over subcutaneous or intramuscular vaccination. First, intranasal vaccines can induce a mucosal IgA antibody response in the upper respiratory tract, promoting protection from influenza virus infection.[1] Second, intranasal vaccination is needle-free. This simplifies the vaccination process and reduces the risk of accidental needle-stick injury. Live attenuated intranasal influenza vaccines have been approved for clinical use; however, these intranasal vaccines can be inoculated to only limited age groups. To apply intranasal influenza vaccines to a wider range of patients, intranasal administration of inactivated influenza vaccines is considered to be a promising strategy in terms of efficacy and safety.[2] However, in general, intranasal inactivated influenza vaccines need adjuvants to induce an adequate immune response.

Synthetic RNA analogues [*e.g.*, poly(I:C)] work as an adjuvant for intranasal inactivated influenza vaccines.[3] The poly(I:C) interacts with several receptors, such as toll-like receptor 3 (TLR3), to trigger innate immune responses.[4] Although it has been reported that only 40–50 base pairs are required for double-stranded RNA (dsRNA) to interact with TLR3,[5,6] the adjuvanticity of poly(I:C)s is strongly dependent on their molecular weight. Poly(I:C)s with a higher molecular weight tend to show not only higher adjuvanticity but also higher toxicity.[7,8] Therefore, low-molecular-weight poly(I:C), which shows less toxicity, is required for clinical use as an adjuvant from the view point of safety. Recently, Nakano *et al.* reported a new synthetic approach to low-molecular-weight (~400 bp) poly(I:C) with a narrow size distribution (Fig. S1†).

[a]*Graduate School of Chemical Sciences and Engineering, Hokkaido University, Sapporo 060-8628, Japan*
[b]*Department of Pathology, National Institute of Infectious Diseases, Toyama 1-23-1, Shinjuku-ku, Tokyo 162-8640, Japan. E-mail: tksuzuki@nih.go.jp*
[c]*Research Center for Zoonosis Control, Hokkaido University, Sapporo 001-0020, Japan*
[d]*School of Medicine, Sapporo Medical University, Sapporo 060-8556, Japan*
[e]*Research Institute for Electronic Science, Hokkaido University, Sapporo 001-0021, Japan*
[f]*Global Station for Soft Matter, Global Institution for Collaborative Research and Education (GI-CoRE), Hokkaido University, Sapporo 001-0021, Japan*
[g]*Technical Research Laboratories, Kyowa Hakko Bio Co., Ltd., Hofu 747-8522,Japan*
[h]*Graduate School of Agriculture, Hokkaido University, Sapporo 060-8589, Japan*
[i]*Global Station for Zoonosis Control, Global Institution for Collaborative Research and Education (GI-CoRE), Hokkaido University, Sapporo 001-0020, Japan*
[j]*Department of Innovative Systems Engineering, Nippon Institute of Technology, 4-1 Gakuendai, Miyashiro-machi, Minamisaitama-gun, Saitama 345-8501, Japan. E-mail: niikura.kenichi@nit.ac.jp*

† Electronic supplementary information (ESI) available. See DOI: 10.1039/c8ra01690a

They found that the annealing of multiple 40-base polyI molecules with a single 400-base polyC molecule produces a double-stranded poly(I:C) with uniform molecular weight distribution. This combination prevents the elongation of dsRNA caused by their linking and enables the use of low-molecular weight poly(I:C) of stable length, reducing its toxicity.[9] This unevenly structured poly(I:C) was referred to as uPIC(40:400). Although this uPIC(40:400) is a promising adjuvant due to its low toxicity, its adjuvanticity remains inadequate.

Nanoparticles are good candidates for use as uPIC(40:400) scaffolds to enhance adjuvanticity. Nanoparticles have already been widely used as vaccine carriers due to their ability to enhance cellular uptake of drugs[10–12] and activate immune systems.[13–20] The immobilization of antigens onto nanoparticles and resultant enhancement of immunogenicity were initially demonstrated in the 1980s.[13] Regarding the targeting of the nasal cavity, antigen delivery using nanogels[21] and polymer nanoparticles[22] has been shown to be effective. Recently, the effects of antigen carrier size and shape have also been investigated as the size and shape of nanoparticles affect both nanoparticle uptake[23–32] and immune responses.[33–39] Plebanski *et al.* reported that the size of the antigen carrier influenced the immune response pathway *in vivo* after intradermal immunization.[33] We previously demonstrated the effects of the shape of the antigen scaffold on vaccine efficacy and cytokine production in mice immunized intraperitoneally.[36] Recently, adjuvant conjugation onto AuNPs and subsequent application to vaccines has been demonstrated. Radovic-Moreno *et al.* reported that the conjugation of CpG oligonucleotides onto AuNPs enabled the adjuvant dose to be decreased while enhancing vaccine potency in systemically immunized mice.[40] Zhang *et al.* reported an enhanced antigen-specific T cell response in mice intradermally immunized with multilayered co-assemblies of antigen and poly(I:C) on AuNPs.[41] Zhou *et al.* demonstrated that there was an optimal size for AuNPs used as an antigen or adjuvant carrier to enhance cellular immunity both *in vitro* and *in vivo*.[39] However, for intranasal vaccines, the influence of the shape and size of the carrier nanomaterial on adjuvanticity has not been explored.

In this study, we aimed to clarify the shape- and size-related effects of AuNPs as scaffolds for uPIC(40:400) adjuvants for the intranasal influenza vaccine through a comparison with conventional subcutaneous vaccination. We chose AuNPs as scaffolds as they were easily synthesized to the desired shape and size compared to other materials. AuNP–uPIC(40:400) complexes (referred to as AuNP–PICs) were obtained by the electrostatic conjugation of uPIC(40:400) onto the AuNP surface. The AuNP–PICs were administrated subcutaneously or intranasally with influenza virus hemagglutinin (HA, 10 or 100 ng). We chose the subcutaneously (SC) administration as a standard reference to intranasal administration in this study. The secreted levels of systemic IgG and mucosal IgA antibodies against influenza virus hemagglutinin (HA) in the serum or nasal wash were evaluated. The activities of the AuNP–PIC adjuvants were further investigated from the virus levels remaining in the nasal wash after challenge infection (Fig. 1). The shape- and size-related effects of the AuNPs were found to be dependent on the administration route and antigen dose. In particular, for intranasal vaccination, the enhanced adjuvanticity of uPIC(40:400) by conjugation with gold nanorods with 10 ng of HA antigen dose was clearly demonstrated.

2. Materials and methods

2.1 Materials

All commercially available reagents were used without further purification. Cetyltrimethylammonium chloride (CTAC), cetyltrimethylammonium bromide (CTAB), hydrogen tetrachloroaurate (III) tetrahydrate, silver nitrate and L(+)-ascorbic acid were purchased from Wako Pure Chemical Industries (Japan). Sodium borohydride was purchased from TOKYO Chemical Industry (Japan). uPIC(40:400) was supplied from Kyowa Hakko Bio (Japan). Poly(I:C) was purchased from GE Healthcare (USA). In this study, we used two different strains of H1N1. Ether-split vaccine of X-179A was kindly provided by the Research Foundation for Microbial Disease of Osaka University (BIKEN, Kanonji, Kagawa, Japan). X-179A is high-growth reassortant vaccine strains

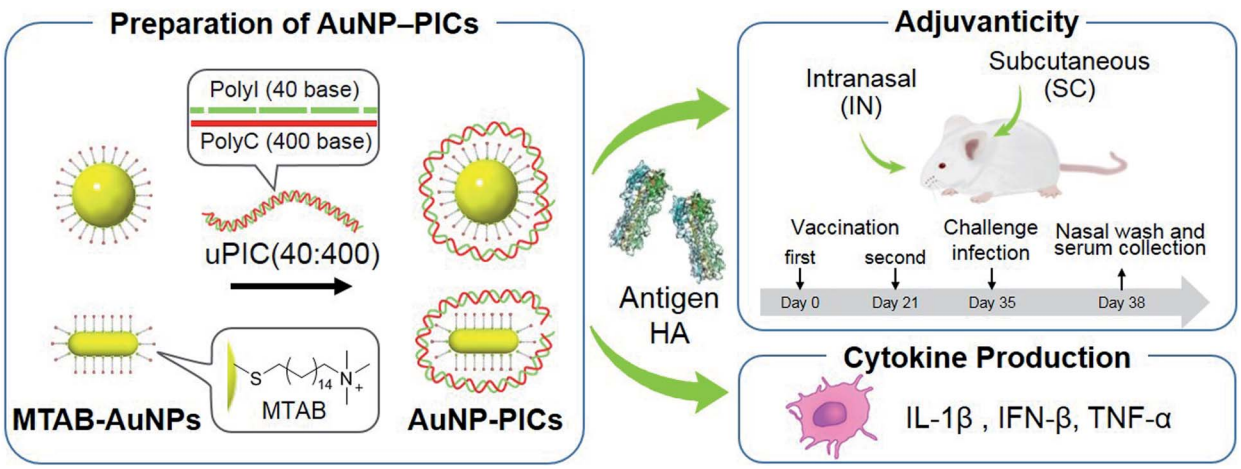

Fig. 1 Preparation of AuNP/uPIC(40:400) conjugates and evaluation of the adjuvanticity and cytokine production.

derived from A/California/7/09 (H1N1)pdm09 for vaccine production in embryonic eggs, and influenza vaccines in clinical use at the time of our animal experiment contained HA antigens of X-179. Mouse-adapted A/Narita/1/09 (H1N1)pdm09 virus, which is not a reassortant strain, was prepared according to the previous report.[42] This strain is derived from a H1N1 pandemic human isolate in 2009, which has the identical antigenicity to A/California/7/09 (H1N1)pdm09 virus. In general, human influenza virus can not replicate efficiently in mice, requiring that mice-adaptation process for mice challenge experiment. The mouse-adapted A/Narita/1/09 (H1N1)pdm09 virus was developed for a mice challenge experiment by our group to test the efficacy of HA vaccines of a H1N1 pandemic virus.[42] Anti-Ms IgA (α) Ab HSA (Biotin) was purchased from KPL (SeraCare Life Sciences, USA). Biotin-SP (long spacer) AffiniPure Goat Anti-Mouse IgG (Fcγ fragment specific) was purchased from Jackson ImmunoResearch (USA). Streptavidin-AP was purchased from Thermo Fisher Scientific (USA). Phosphatase substrate was purchased from Sigma-Aldrich (USA). BALB/c mice were purchased from Japan SLC (Japan). C3H/HeNJcl mice were purchased from Hokudo (Japan). Dulbecco's modified Eagle's medium (DMEM), RPMI-1640 and lipopolysaccharides (LPS) were purchased from Sigma-Aldrich (USA). DMEM (no phenol red), fetal bovine serum (FBS) and penicillin–streptomycin were purchased from GIBCO (USA). Recombinant murine GM-CSF was purchased from PEPROTECH (USA). Cell Counting Kit-8 was purchased from DOJINDO (Japan). Interleukin-1β (IL-1β) and tumor necrosis factor-α (TNF-α) ELISA kits were purchased from R&D systems (USA). Interferon-β (IFN-β) ELISA kit was purchased from PBL Assay Science (USA).

2.2 AuNP–PIC preparation

Cetyltrimethylammonium (CTA)-stabilized AuNPs were synthesized by a seeding growth method as described previously.[43,44] The surface of the AuNPs was functionalized by MTAB as synthesized according to a previous report.[45] After residual MTAB molecules were removed by centrifugation, MTAB-AuNPs were added to uPIC(40:400) solution reconstituted in distilled water and mixed gently.

2.3 Evaluation of AuNP–PIC adjuvanticity

2.3.1 Vaccination. Six- to eight-week-old female BALB/c mice (n = 5–6 per group) were immunized intranasally or subcutaneously twice at a 3-week interval with 100 or 10 ng of ether-split influenza vaccine made from vaccine strain X-179A, derived from A/California/7/09 (H1N1)pdm09, in the presence of AuNPs alone, AuNP–PICs or uPIC(40:400). Intranasal vaccination was performed by instillation of 5 μL of vaccine solution into each nostril (total 10 μL per mouse). Subcutaneous vaccination was performed by injection of 100 μL of vaccine solution into the dorsal part of the cervical region.[46,47] All mice were challenged with mouse-adapted A/Narita/1/09 (H1N1)pdm09 virus (A/NRT), 2 weeks after the last vaccination. Infection was performed by inserting 2 μL of a suspension containing A/NRT in each nostril (total 4 μL, 40 000 plaque-forming units [PFUs] per mouse). At 3 days post-infection, all mice were sacrificed to collect serum and nasal wash samples for determination of antibody levels and virus titers as previously described. Nasal wash specimens were obtained from mice by washing the nasal cavity of the isolated upper head with 1 mL of PBS(−) containing 0.1% bovine serum albumin and antibiotics.[48] In the experiments on intranasal immunization, we also checked the virus titers as well as antibody responses, which correspond to the levels of virus replication in the nasal mucosal tissues in the vaccinated animals after virus challenge infection. All immunizations and infections were performed under anesthesia. These animal experiments were conducted in strict compliance with animal husbandry and welfare regulations in handled in biosafety level two animal facilities according to the guidelines of the Animal Care and Use Committee of the National Institute of Infectious Diseases, and were approved by this Committee.

2.3.2 Evaluation of antibody response. Hemagglutinin (HA)-specific IgG and IgA antibodies in serum or nasal wash samples were quantified by enzyme-linked immunosorbent assay (ELISA). Recombinant trimeric HA, produced by the method of Stevens *et al.*,[49] was used as the coating antigen. HA-specific IgA antibodies were detected using biotin-conjugated goat anti-mouse IgA antibodies (Kirkegaard & Perry Laboratories, USA) and alkaline phosphatase-conjugated streptavidin (Thermo Fisher Scientific, USA). The detection reaction was initiated by the addition of *p*-nitrophenylphosphate (Sigma-Aldrich, USA) in 10 mM diethanolamine (pH: 9.8) containing 0.5 mM $MgCl_2$. Absorbance at 405 nm was measured using an iMark Microplate Reader (BIO-RAD, Hercules, USA). Pooled nasal wash samples collected from hyperimmune mice was used as a standard for the quantification of nasal IgA. ELISA was performed using serial two-fold dilutions of standard serum and nasal wash (NW) (from 1 : 100 and 1 : 1, respectively) as described above. The reciprocal of highest dilution rate of sample showing positive reaction was defined as ELISA unit. The threshold value for positive reaction was defined as mean ± 3SD of serially diluted serum or NW samples collected from a non-vaccinated BALB/c mouse.

2.3.3 Measurement of virus titers. Virus titers in the nasal wash specimens were measured according to a previously described method.[50] Briefly, 200 μL aliquots of serial 10-fold dilutions of the nasal wash were inoculated into Madin–Darby canine kidney (MDCK) cells in a six-well plate. After allowing the plates to incubate for 1 h, each well was overlaid with 2 mL of agar medium. The number of plaques was counted following crystal violet staining at 2 days after inoculation.

2.4 Cytotoxicity assay and cytokine production measurement

Murine bone marrow-derived dendritic cells (BMDCs) were prepared according to a previously reported method.[51] These animal procedures were performed in accordance with the Guidelines for Care and Use of Laboratory Animals of Hokkaido University and approved by the Animal Ethics Committee of Hokkaido University. For the evaluation of IL-1β production, the collected BMDCs were primed with 50 ng mL^{-1} LPS for 3 h, and then used without purification. BMDCs were mixed with the adjuvant in RPMI-1640 supplemented with 10% FBS,

100 U mL^{-1} penicillin, 100 μg mL^{-1} streptomycin, 25 mM HEPES-KOH and 50 μM 2-mercaptoethanol. The BMDCs were then seeded at 1.0×10^5 cells per well in a 96-well plate with adjuvants. After incubation for 24 h, culture supernatants were collected to measure cytokine concentration and cells were washed twice with culture medium supplemented with 10% FBS, 100 U mL^{-1} penicillin, 100 μg mL^{-1} streptomycin and 25 mM HEPES-KOH. Cellular viabilities were evaluated using a Cell Counting Kit-8 (CCK-8). After incubation with CCK-8, the absorbance at 450 nm was measured using a microplate reader (infinite 200 PRO, Tecan, Switzerland). The concentrations of IL-1β, IFN-β and TNF-α in the culture supernatant were determined by ELISA following the manufacturer's protocols.

2.5 Statistics

Statistical analysis was performed using the GraphPad Prism statistical software package (Version 7.01: Graph Pad Software Inc., USA). The threshold for statistical significance was set at 5% ($p < 0.05$).

3. Results and discussion

3.1 Preparation of AuNP–PICs

Spherical and rod-shaped gold nanoparticles were synthesized *via* conventional seeding growth methods.[44,52] Synthesized cetyltrimethylammonium (CTA)-stabilized AuNPs were functionalized with (16-mercaptohexadecyl)trimethylammonium bromide (MTAB) as MTAB functionalization provides a cationic surface with lower cytotoxicity compared to CTA-stabilized AuNPs due to the removal of excess surfactant.[45] The average size of the MTAB-functionalized AuNPs (MTAB-AuNPs) was determined from transmission electron microscope (TEM) images by counting at least 100 particles (Fig. 2). The mean diameters of the spherical AuNPs were 20 ± 0.9 and 41 ± 2.2 nm. The mean lengths and diameters of the rod-shaped AuNPs were 28 ± 3.2 × 7.9 ± 0.9 and 41 ± 4.8 × 12 ± 1.6 (core size in Table 1). Here, these MTAB-functionalized spherical AuNPs are referred to as Sphere20 and Sphere40, and the MTAB-functionalized rod-shaped AuNPs are referred to as Rod30 and Rod40 in accordance with their shape and size.

MTAB-AuNPs were added to uPIC(40:400) solutions, affording the AuNP–uPIC(40:400) complexes (referred to as Sphere20-PIC, Sphere40-PIC, Rod30-PIC and Rod40-PIC, respectively). To standardize the uPIC(40:400) dose, the resultant AuNP–PICs were used without purification. Conjugation of uPIC(40:400) onto the AuNPs was confirmed by changes in zeta-potentials from positive (39–64 mV) to negative (−47 to −53 mV). For example, the zeta potential of Sphere20 was changed from 39 mV to −53 mV after addition to the uPIC(40:400) solution (Table 1). The colloidal dispersibility in solution of the various AuNP–PICs was examined by extinction spectra. The extinction spectra of the AuNPs did not change after mixing with uPIC(40:400) in water (Fig. S2†), indicating that the AuNPs did not aggregate after coating with uPIC(40:400) molecules. The number of immobilized uPIC(40:400) molecules on a single AuNP was quantified from the concentration of unbound uPIC(40:400) in the supernatant after centrifugation. The average number of uPIC(40:400) molecules attached on a single particle ranged from 5.2 to 20 molecules (Table 1). For the vaccination, the AuNP–PICs were mixed with hemagglutinin. We, therefore, investigated whether HA was attached onto the AuNP–PICs using dynamic light scattering (DLS). The hydrodynamic diameter of the AuNP–PICs after mixing with HA did not change (Fig. S3†), whereas positively charged MTAB-AuNPs showed a large shift in the DLS peak after mixing with HA (Fig. S4†). This difference suggests that the interaction of HA with the AuNP–PICs is so weak that it can be ignored and that the AuNP–PICs do not work as a delivery carrier of antigen HA. For the *in vitro* study, the AuNP–PICs were applied to the culture media. Thus, we investigated their colloidal dispersibility in the culture media. All AuNP–PICs, except Rod30-PIC, showed good dispersibility in the culture media (Fig. S5†).

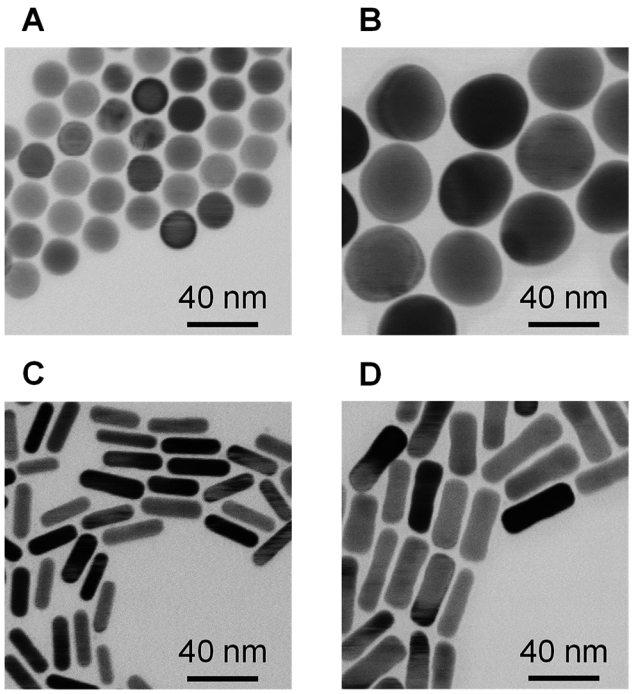

Fig. 2 TEM images of MTAB-AuNPs. (A) Sphere20, (B) Sphere40, (C) Rod30 and (D) Rod40.

3.2 Adjuvanticity of AuNP–PICs

The AuNP–PICs were administrated subcutaneously or intranasally to mice twice at a 3-week interval with an inactivated split influenza vaccine containing partially purified influenza HA antigens obtained by disruption of influenza virus virions by treatment with ether solvent. Two weeks after the second vaccination, mice were challenged with influenza A virus (A/NRT). The nasal wash and serum samples were then collected at 3 days post-infection to evaluate virus titers, and systemic and mucosal antibody responses in mice (Fig. 1). For vaccination, AuNP conjugations with a total of 10 or 1.0 μg (corresponding to *ca.* 40 and 4 pmol, respectively) of uPIC(40:400)/head were administrated as the adjuvant. The AuNP–PIC solutions were

Table 1 Physicochemical properties of the AuNP–PICs (means ± SD)

	Size of core[a] [nm]	Zeta potential[b] [mV]	Surface area of core [nm^2]	Number of uPIC (40:400)/particle[b]
Sphere20-PIC	20 ± 0.9	−53 ± 6.7	1300	5.2 ± 0.2
Sphere40-PIC	41 ± 2.2	−48 ± 4.8	5000	12 ± 0.1
Rod30-PIC	28 ± 3.2 × 7.9 ± 0.9	−47 ± 5.3	770	20 ± 1.1
Rod40-PIC	41 ± 4.8 × 12 ± 1.6	−49 ± 2.1	1800	10 ± 1.0

[a] Nanoparticle sizes were determined from at least 100 particles in TEM images. [b] Zeta potentials of the AuNP–PICs and the number of immobilized uPIC(40:400) molecules were determined from at least 3 independent experiments.

finally administrated soon after mixing with an aqueous solution containing 100 or 10 ng of HA antigens.

First, we evaluated IgG antibody responses in mice immunized with 100 ng of HA subcutaneously, as this is commonly used to assess vaccine-induced immune response. Commercially available poly(I:C) was used as a positive control. No significant difference was observed between the AuNP–PIC groups and uPIC(40:400). On the other hand, in comparison with the negative control (top bar in Fig. 3A left), all AuNP–PIC groups showed significant responses, whereas uPIC(40:400) and poly(I:C) did not (Fig. 3A left). Although uPIC(40:400), the AuNP–PICs and poly(I:C) seemed to show similar IgG responses, a trend toward higher IgG responses in the AuNP–PIC groups were observed.

The adjuvanticity of the AuNP–PICs for the intranasal vaccine was then evaluated. Before intranasal immunization, we observed Sphere40-PIC and Rod40-PIC uptake in the nasal epithelium. Fig. 4 showed TEM images of tissue sections of the nasal epithelium after intranasal immunization. Both Sphere40-PICs and Rod40-PICs were found among the cilia and

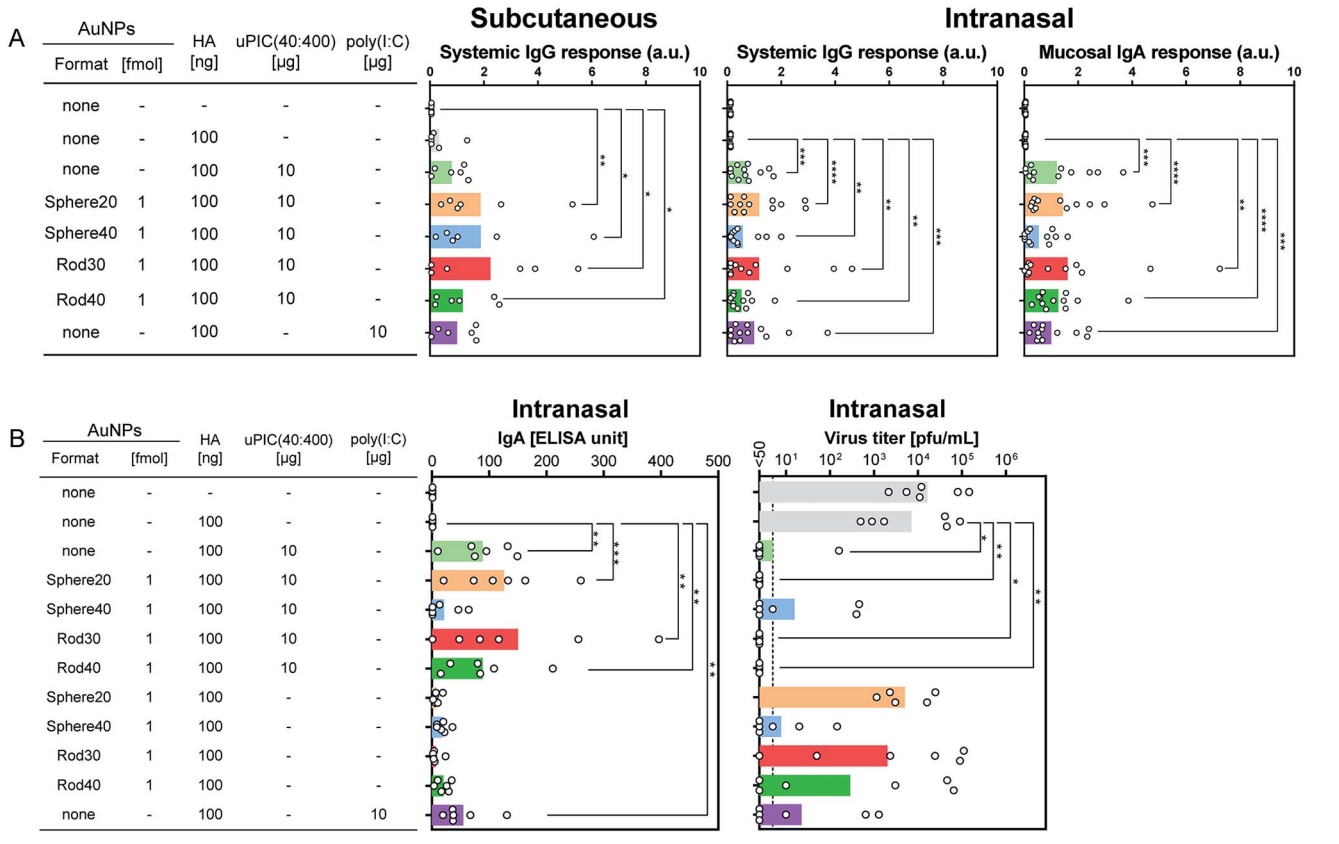

Fig. 3 (A) Antibody production in mice immunized with 100 ng of antigen HA (X-179A ether-split vaccine) combined with adjuvants subcutaneously (SC; left) or intranasally (IN; center, right). For the IN immunization, two independent experiments were carried out (n = 5–6 in each experiment). Data were normalized against the poly(I:C) group. These normalized values were shown as arbitrary units (a.u.). Regarding the intranasal immunization shown (A), two independent experiments were carried out. Average values of antibody responses were obtained from normalized data against the poly(I:C) group in each experiment. (B) Negative correlations between HA-specific IgA antibodies and viral loads in nasal wash samples. Each circle represents an individual titer, and each bar represents the mean of IgA ELISA units and the geometric mean titer of the virus titers. The dotted line indicates 50 pfu mL^{-1} of virus titer, which was the detection limit. Statistical analysis was performed using Kruskal–Wallis tests with Dann's multiple comparison tests. The asterisks *, **, *** and **** indicate $p < 0.05$, $p < 0.01$, $p < 0.001$ and $p < 0.0001$, respectively.

in the cellular vesicles in the nasal epithelium, indicating that, regardless of the shape of the AuNPs, AuNP–PICs can reach the cells located in the nasal epithelium *via* intranasal immunization, although their efficiencies remain unclear. Then, intranasal immunization was conducted using the same dose as the subcutaneous immunization to evaluate systemic IgG and mucosal IgA responses. Unlike the subcutaneous immunization, uPIC(40:400) itself showed a significant adjuvant effect on IgG antibody response. Significant IgG antibody responses were also confirmed for all AuNP–PIC groups (Fig. 3A center). With regard to the IgA response to the intranasal immunization, all uPIC(40:400), poly(I:C) and AuNP–PIC groups showed significant responses, except for Sphere40-PIC, in comparison to the response induced by HA alone (Fig. 3A right). Thus, for the intranasal immunization using 100 ng HA antigens, we concluded that all AuNP–PIC groups except for Sphere40-PIC showed the same level of adjuvanticity as uPIC(40:400) and poly(I:C). Interestingly, Sphere40-PICs demonstrated a negative effect when used for intranasal immunization, despite the positive effect observed for subcutaneous vaccination. This indicates that the shape and size of the adjuvant scaffold should be optimized according to the vaccine administration route.

To protect from influenza virus infection, mucosal IgA antibody against the virus is particularly crucial.[1] In one set of experiments (n = 5–6) on intranasal immunization, we also checked the virus titers as well as antibody responses, which correspond to the virus levels remaining in the nasal wash after challenge infection. The groups showing higher mucosal IgA antibody responses tended to show lower virus titers (Fig. 3B). This good correlation between mucosal IgA antibody responses and virus titers indicates that the induced IgA antibodies play a principal role in protecting against viral infection.

For intranasal vaccination, the administration of a high dose (100 ng HA) suppressed the virus titer too efficiently as shown in Fig. 3B to evaluate differences in adjuvanticity among the AuNP–PICs. Thus, the administration level of HA was reduced to 10 ng to allow better evaluation of adjuvanticity using virus titers. When Rod30-PICs and Rod40-PICs with 10 ng of HA antigen were used, significantly higher adjuvanticity was observed in comparison to uPIC(40:400), while Sphere40-PICs did not show significant adjuvanticity (Fig. 5 left). As a control, Rod30 and Rod40 without uPIC(40:400) did not induce any reduction in the viral titer (Fig. 5 left), indicating that the gold nanorods themselves did not demonstrate any

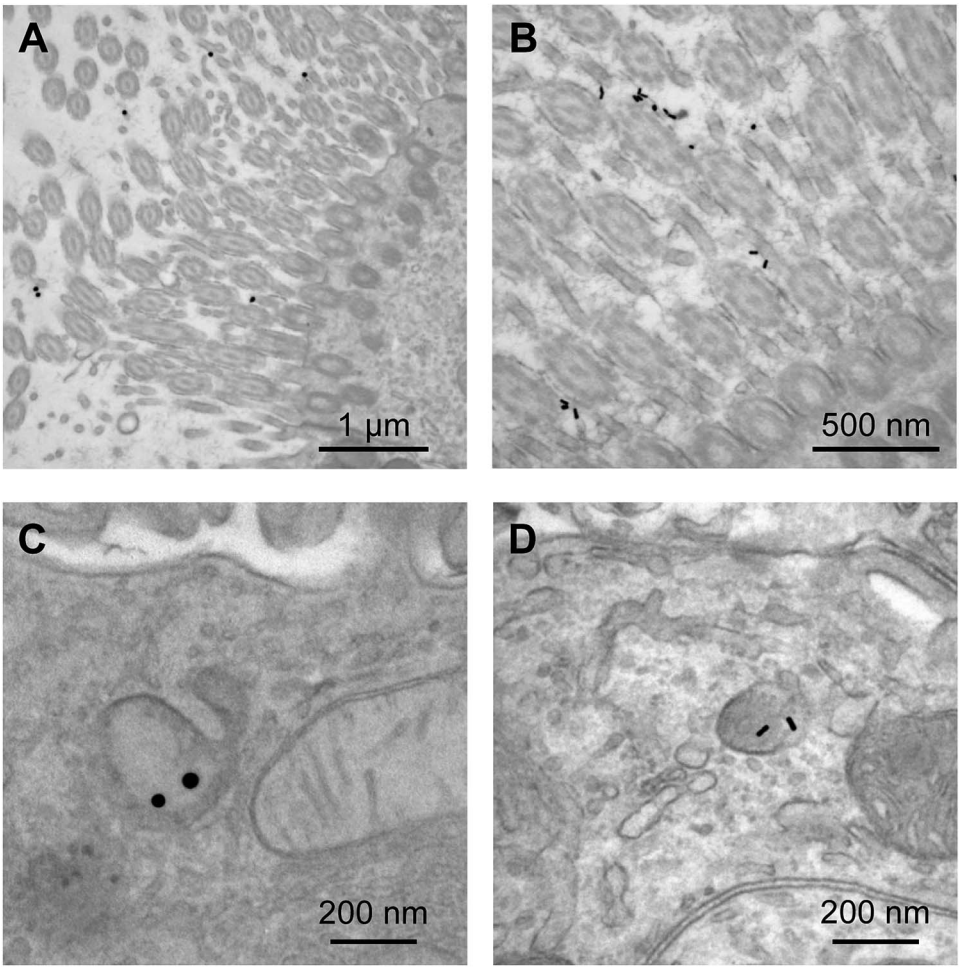

Fig. 4 TEM images of nasal epithelial tissue from mice administrated Sphere40-PICs (A and C) or Rod40-PICs (B and D) intranasally.

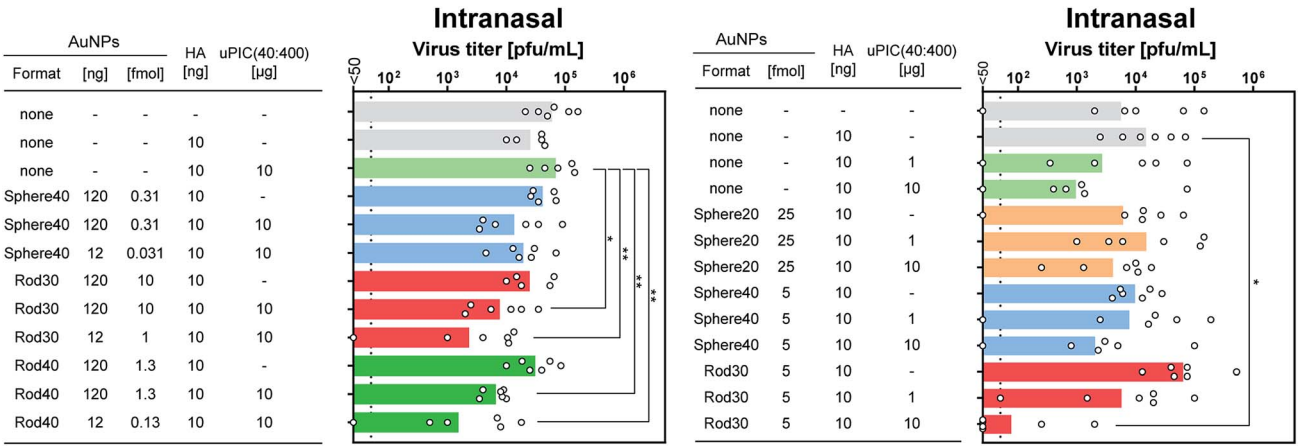

Fig. 5 The reduction of viral loads in nasal wash samples from mice immunized intranasally with 10 ng of HA. Each circle and bar represents the individual titer and geometric mean titer, respectively. The dotted line indicates 50 pfu mL^{-1} of virus titer which is the detection limit. Statistical analysis was performed using Kruskal–Wallis tests with Dann's multiple comparison tests. The asterisks *and ** indicate $p < 0.05$ and $p < 0.01$, respectively.

adjuvanticity under these conditions. Fig. 5 shows that the lower doses (12 ng AuNPs) of Rod30-PIC and Rod40-PIC are more effective in reducing the viral titer than the higher doses (120 ng AuNPs). Although the reason for this is unclear, we assume that there might be an optimal amount of adjuvant for the induction of effective immune responses. The protection from viral infection with a lower adjuvant dose is preferable as it minimizes the risk of adverse reactions. On the other hand, no significant differences between Sphere20-PICs or Sphere40-PICs and uPIC(40:400) alone were observed when 10 ng of HA antigen was used (Fig. 5 right). These results clearly show that uPIC(40:400) adjuvanticity was enhanced by conjugation with Rod30s and Rod40s rather than with Sphere20s or Sphere40s at a lower range of HA doses, thereby demonstrating a shape-related effect on intranasal vaccination.

These *in vivo* studies newly demonstrate two points: (1) the shape-related effect of the adjuvant scaffold is dependent on the administration route, and (2) rod-shaped nanoparticles are effective as a scaffold for RNA adjuvants for intranasal vaccines at low antigen doses.

3.3 Cytokine production from BMDCs treated with AuNP–PICs

Cytokines are a key mediator in the induction of immune responses. However, excess cytokine production can cause various adverse effects.[53–55] When attempting to enhance the adjuvanticity of uPIC(40:400), it is important to avoid excess cytokine production which can lead to toxicity.[56] Further, it was expected that the information obtained on cytokine production could provide some sights into mechanisms associated with *in vivo* adjuvanticity. Thus, we evaluated cellular viability and the production of three cytokines; IL-1β, IFN-β and TNF-α. Commercially available poly(I:C) and alum, a TLR3 agonist and an inflammasome activator, respectively, were used as positive controls.

First, we checked cellular viability using a Cell Counting Kit-8 (CCK-8) after incubation with AuNP–PICs for 24 h. When BMDCs were stimulated with 10 μg mL^{-1} of poly(I:C), a significant reduction in viability, which was comparable to that induced by 200 μg mL^{-1} of alum, was observed. On stimulation by the AuNP–PIC groups, BMDC viabilities were maintained compared to the uPIC(40:400) group (Fig. 6A), supporting the notion that the AuNP–PICs did not cause cellular damage *in vitro*.

IL-1β is a major mediator of the innate immune system and inflammation.[57] Various particles are known to induce IL-1β production, such as amino-functionalized nanoparticles,[15] rod-shaped particles with a high aspect ratio[58,59] and larger-sized particles.[60] In our experiment, increased IL-1β production was induced by Sphere40-PICs, but not by Sphere20-PICs, Rod30-PICs or Rod40-PICs (Fig. 6B). This result indicates the Rod30-PICs and Rod40-PICs did not cause lysosomal rupture. We assumed that Sphere40-PICs induced the highest level of IL-1β production as Sphere40-PICs have the largest volume among the tested particles, thereby causing some damage to the lysosome.

IFNs and pro-inflammatory cytokines are secreted upon stimulation by dsRNAs.[4] The level of IFN-β production was somewhat increased by the conjugation of uPIC(40:400) with Sphere40s, and slightly increased by that with Rod30s (Fig. 6C). Rod30-PICs at the highest AuNP concentration tended to aggregate in the medium (Fig. S3†). This aggregation may affect IFN-β production through particle size enlargement. Interestingly, when compared to poly(I:C), uPIC(40:400) and AuNP–PICs induced little IFN-β production. This suggests that the AuNP–PICs may elicit the immune responses through a pathway that is not dependent on TLR3, in other words, the conjugation of uPIC to AuNPs may affect the immune routes. Further, Sphere40-PICs with 200 and 400 pM of AuNPs induced higher levels of IFN-β production than did uPIC(40:400). As Sphere40-PICs showed higher IL-1β induction, which can be caused by lysosomal

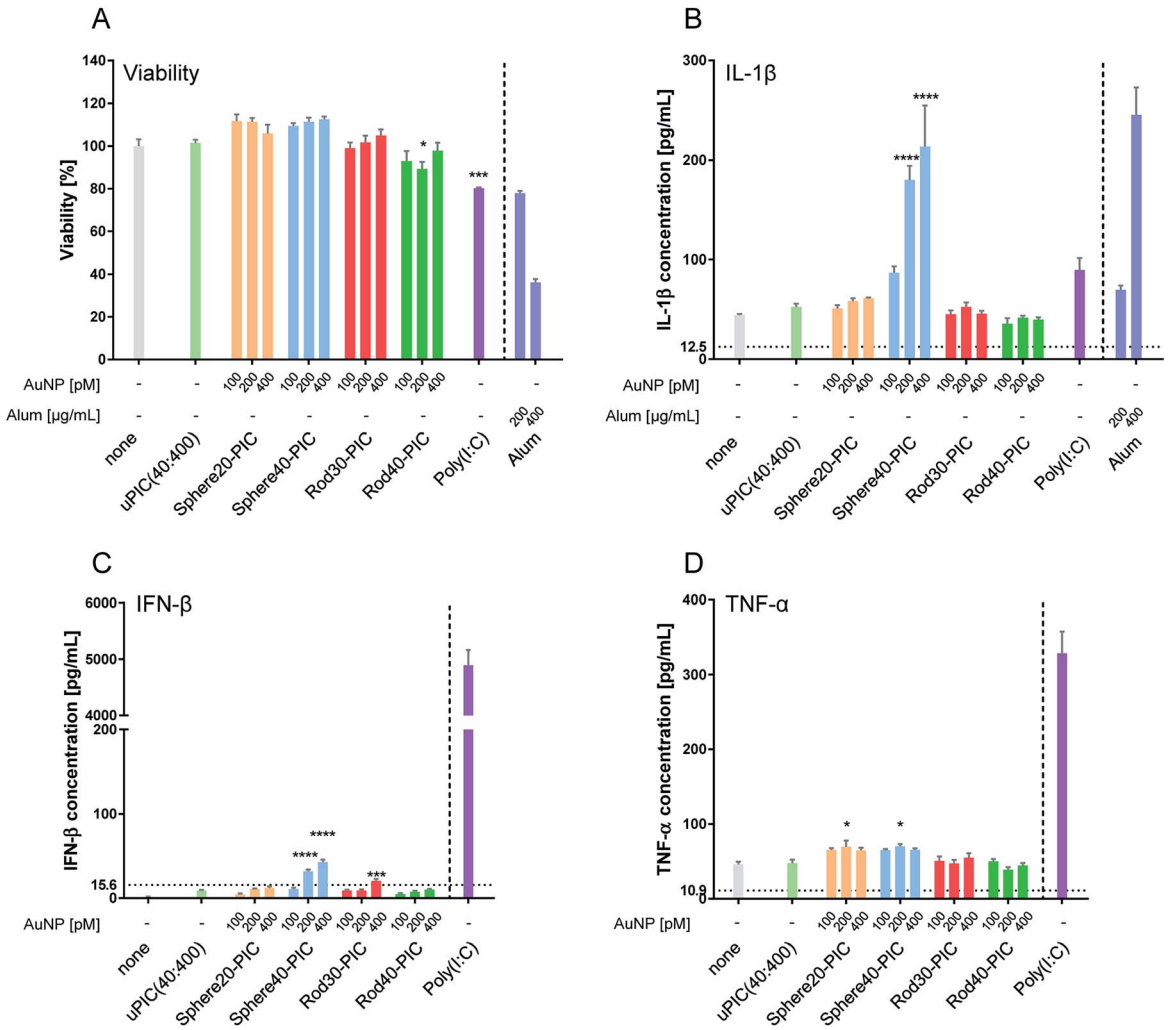

Fig. 6 (A) Cellular viability of BMDCs treated with AuNP–PICs containing 10 μg mL^{-1} of uPIC(40:400) final concentration for 24 h at 37 °C (means ± SEM, $n = 3$). (B) IL-1β, (C) IFN-β and (D) TNF-α production from BMDCs treated with AuNP–PICs for 24 h at 37 °C. For the evaluation of IL-1β production, BMDCs were primed with 50 ng mL^{-1} of LPS for 3 h. Alum and poly(I:C) were used as positive controls. The detection limit is indicated by the horizontal dotted line. Statistical analysis was performed against uPIC(40:400)-treated BMDC groups using one-way ANOVA tests with Dunnett's multiple comparison tests. Positive controls (right side of the vertical dotted line) were excluded from the statistical analysis. The asterisks *, **, *** and **** indicate $p < 0.05$, $p < 0.01$, $p < 0.001$ and $p \leq 0.0001$, respectively.

rupture, Sphere40-PICs may induce IFN-β production through activation of RIG-I-like receptors[4] in the cytoplasm.

We next checked the production of TNF-α, a representative pro-inflammatory cytokine that plays a role in host defense against infection. Treatment with uPIC(40:400) alone, Rod30-PICs and Rod40-PICs induced almost no enhancement of TNF-α production, whereas slight levels of TNF-α were induced by incubation with Sphere20-PICs and Sphere40-PICs (Fig. 6D). Additionally, as antigen immunogenicity has been reported to be enhanced by conjugation with nanoparticles,[36] we tested whether the HA antigen affects cytokine production when stimulated with AuNP–PICs. No changes in IFN-β or TNF-α production were observed for the AuNP–PIC groups in the presence of HA antigen, indicating that the induction of cytokine production by the AuNP–PICs was not influenced by the presence of HA antigens (Fig. S6†).

In the *in vitro* experiments, Rod30-PICs and Rod40-PICs induced low levels of cytokine production while Sphere40-PICs tended to induce inflammatory cytokine production. Since this tendency does not correlate with adjuvanticity observed for *in vivo* vaccination, we cannot identify the detailed mechanism based only on the cytokine production. Importantly, however, the low levels of inflammatory cytokine induction by Rod30-PICs and Rod40-PICs are helpful in avoiding the adverse reactions originating from excess cytokine production. Therefore, the rod-shaped gold nanoparticle/uPIC(40:400) complexes appear to be good potential adjuvants for the development of intranasal inactivated influenza vaccines with fewer side effects.

4. Conclusion

In summary, we investigated the influence on adjuvanticity of the shape and size of AuNPs as scaffolds for the immobilization

of uPIC(40:400) through a comparison of intranasal and subcutaneous administration. For the subcutaneous vaccination, IgG antibody responses were slightly enhanced by conjugation with AuNPs, and the effect of the AuNP shape on the systemic IgG responses was limited for all tested AuNP–PICs. On the other hand, for the intranasal vaccination at a lower HA dose, Rod30-PICs and Rod40-PICs clearly suppressed viral infection while Sphere20-PICs and Sphere40-PICs did not. In *in vitro* experiments, Rod30-PICs and Rod40-PICs did not increase inflammatory cytokine production, which is known to be a potential cause of adverse reactions. From these results, we concluded that the shape-related effect of AuNPs is dependent on the immunization route, and gold nanorods afford an effective adjuvant scaffold for uPIC(40:400) as an intranasal influenza vaccine. Our findings indicate that utilizing shape-controlled nanoparticles as scaffolds for adjuvant molecules is a good approach to enhance weak adjuvanticity without resulting in excessive inflammatory responses. In other words, the appropriate choice of nanomaterial shape could be crucial to the design of safe and effective intranasal inactivated vaccines. More comprehensive studies of nanoparticles are expected to reveal further applications.

Author contributions

T. T., T. S. and K. N. conceived this theme and wrote the manuscript. H. M., T. N., H. H., K. I. and H. S. provided insights to the theme design. T. N. prepared uPIC(40:400). T. T. performed the synthesis and characterization of AuNP–PICs. K. T., A. A., Y. O., H. H. and T. S. performed *in vivo* experiments and evaluation of IgA production and virus titer. T. T., S. K. and Y. O. conducted BMDC preparation and *in vitro* experiments. T. N. conducted TEM observation of nasal tissue section.

Conflicts of interest

There are no conflicts to declare.

Acknowledgements

This work was supported by the Canon Foundation and JSPS KAKENHI 16H03822. A part of this work was supported by the Nanotechnology Platform Program of MEXT. The work described in this report was partially supported by the Research Program on Emerging and Re-emerging Infectious Diseases (Grant Number JP18fk0108012j0003 and JP18fk0108051j0302), the Japan Initiative for Global Research on Infectious Diseases (J-GRID) of Japan from the Japan Agency for Medical Research and Development, AMED (JP18fm0108008). We thank Ms K. Sano for her help in the measurement of virus titers. Zeta potential measurements were carried out at the OPEN FACILITY, Hokkaido University, Sousei Hall.

References

1 H. Asanuma, J. Ohori, J. McGhee and K. Fujihashi, *Clin. Immunol., Endocr. Metab. Drugs*, 2015, **2**, 13–26.
2 K. Sano, A. Ainai, T. Suzuki and H. Hasegawa, *Vaccine*, 2017, **35**, 5388–5395.
3 T. Ichinohe, I. Watanabe, S. Ito, H. Fujii, M. Moriyama, S. Tamura, H. Takahashi, H. Sawa, J. Chiba, T. Kurata, T. Sata and H. Hasegawa, *J. Virol.*, 2005, **79**, 2910–2919.
4 C. J. Desmet and K. J. Ishii, *Nat. Rev. Immunol.*, 2012, **12**, 479–491.
5 J. N. Leonard, R. Ghirlando, J. Askins, J. K. Bell, D. H. Margulies, D. R. Davies and D. M. Segal, *Proc. Natl. Acad. Sci. U. S. A.*, 2008, **105**, 258–263.
6 L. Liu, I. Botos, Y. Wang, J. N. Leonard, J. Shiloach, D. M. Segal and D. R. Davies, *Science*, 2008, **320**, 379–381.
7 H. Machida, A. Kuninaka and H. Yoshino, *Jpn. J. Microbiol.*, 1976, **20**, 71–76.
8 K. Kanaya, K. Kondo, K. Suzukawa, T. Sakamoto, S. Kikuta, K. Okada and T. Yamasoba, *Cell Tissue Res.*, 2014, **357**, 279–299.
9 T. Nakano and E. Yamatora, WO 2014088087 A1, 2014.
10 D. A. Giljohann, D. S. Seferos, A. E. Prigodich, P. C. Patel and C. A. Mirkin, *J. Am. Chem. Soc.*, 2009, **131**, 2072–2073.
11 C. H. J. Choi, L. Hao, S. P. Narayan, E. Auyeung and C. A. Mirkin, *Proc. Natl. Acad. Sci. U. S. A.*, 2013, **110**, 7625–7630.
12 K. Niikura, K. Kobayashi, C. Takeuchi, N. Fujitani, S. Takahara, T. Ninomiya, K. Hagiwara, H. Mitomo, Y. Ito, Y. Osada and K. Ijiro, *ACS Appl. Mater. Interfaces*, 2014, **6**, 22146–22154.
13 S. Shiosaka, H. Kiyama, A. Wanaka and T. Masaya, *Brain Res.*, 1986, **382**, 399–403.
14 Y. S. Chen, Y. C. Hung, I. Liau and G. S. Huang, *Nanoscale Res. Lett.*, 2009, **4**, 858–864.
15 O. Lunov, T. Syrovets, C. Loos, G. U. Nienhaus, V. Mailänder, K. Landfester, M. Rouis and T. Simmet, *ACS Nano*, 2011, **5**, 9648–9657.
16 L. Zhao, A. Seth, N. Wibowo, C. X. Zhao, N. Mitter, C. Yu and A. P. J. Middelberg, *Vaccine*, 2014, **32**, 327–337.
17 D. J. Irvine, M. C. Hanson, K. Rakhra and T. Tokatlian, *Chem. Rev.*, 2015, **115**, 11109–11146.
18 Y. Liu, Y. L. Balachandran, D. Li, Y. Shao and X. Jiang, *ACS Nano*, 2016, **10**, 3589–3596.
19 K. T. Gause, A. K. Wheatley, J. Cui, Y. Yan, S. J. Kent and F. Caruso, *ACS Nano*, 2017, **11**, 54–68.
20 L. A. Dykman and N. G. Khlebtsov, *Chem. Sci.*, 2017, **8**, 1719–1735.
21 T. Nochi, Y. Yuki, H. Takahashi, S. Sawada, M. Mejima, T. Kohda, N. Harada, I. G. Kong, A. Sato, N. Kataoka, D. Tokuhara, S. Kurokawa, Y. Takahashi, H. Tsukada, S. Kozaki, K. Akiyoshi and K. Hiroshi, *Nat. Mater.*, 2010, **9**, 572–578.
22 K. Matsuo, H. Koizumi, M. Akashi, S. Nakagawa, T. Fujita, A. Yamamoto and N. Okada, *J. Controlled Release*, 2011, **152**, 310–316.
23 B. D. Chithrani and W. C. W. Chan, *Nano Lett.*, 2007, **7**, 1542–1550.
24 R. Vácha, F. J. Martinez-Veracoechea and D. Frenkel, *Nano Lett.*, 2011, **11**, 5391–5395.

25 J. L. Perry, K. P. Herlihy, M. E. Napier and J. M. DeSimone, *Acc. Chem. Res.*, 2011, **44**, 990–998.
26 A. Albanese, P. S. Tang and W. C. W. Chan, *Annu. Rev. Biomed. Eng.*, 2012, **14**, 1–16.
27 Y. Li, M. Kröger and W. K. Liu, *Nanoscale*, 2015, **7**, 16631.
28 X. Chen, Y. Yan, M. Müllner, Y. Ping, J. Cui, K. Kempe, C. Cortez-Jugo and F. Caruso, *Biomacromolecules*, 2016, **17**, 1205–1212.
29 K. Nambara, K. Niikura, H. Mitomo, T. Ninomiya, C. Takeuchi, J. Wei, Y. Matsuo and K. Ijiro, *Langmuir*, 2016, **32**, 12559–12567.
30 Y. Liu, B. Workalemahu and X. Jiang, *Small*, 2017, **13**, 1701815.
31 C. Kinnear, T. L. Moore, L. Rodriguez-Lorenzo, B. Rothen-Rutishauser and A. Petri-Fink, *Chem. Rev.*, 2017, **117**, 11476–11521.
32 C. G. Uhl, Y. Gao, S. Zhou and Y. Liu, *RSC Adv.*, 2018, **8**, 8089–8100.
33 P. L. Mottram, D. Leong, B. Crimeen-Irwin, S. Gloster, S. D. Xiang, J. Meanger, R. Ghildyal, N. Vardaxis and M. Plebanski, *Mol. Pharm.*, 2007, **4**, 73–84.
34 E. Hutter, S. Boridy, S. Labrecque, M. Lalancette-Hébert, J. Kriz, F. M. Winnik and D. Maysinger, *ACS Nano*, 2010, **4**, 2595–2606.
35 M. F. Bachmann and G. T. Jennings, *Nat. Rev. Immunol.*, 2010, **10**, 787–796.
36 K. Niikura, T. Matsunaga, T. Suzuki, S. Kobayashi, H. Yamaguchi, Y. Orba, A. Kawaguchi, H. Hasegawa, K. Kajino, T. Ninomiya, K. Ijiro and H. Sawa, *ACS Nano*, 2013, **7**, 3926–3938.
37 Y. Liu, Y. Xu, Y. Tian, C. Chen, C. Wang and X. Jiang, *Small*, 2014, **10**, 4505–4520.
38 S. Kumar, A. C. Anselmo, A. Banerjee, M. Zakrewsky and S. Mitragotri, *J. Controlled Release*, 2015, **220**, 141–148.
39 Q. Zhou, Y. Zhang, J. Du, Y. Li, Y. Zhou, Q. Fu, J. Zhang, X. Wang and L. Zhan, *ACS Nano*, 2016, **10**, 2678–2692.
40 A. F. Radovic-Moreno, N. Chernyak, C. C. Mader, S. Nallagatla, R. S. Kang, L. Hao, D. A. Walker, T. L. Halo, T. J. Merkel, C. H. Rische, S. Anantatmula, M. Burkhart, C. A. Mirkin and S. M. Gryaznov, *Proc. Natl. Acad. Sci. U. S. A.*, 2015, **112**, 3892–3897.
41 P. Zhang, Y.-C. Chiu, L. H. Tostanoski and C. M. Jewell, *ACS Nano*, 2015, **9**, 6465–6477.
42 A. Ainai, H. Hasegawa, M. Obuchi, T. Odagiri, M. Ujike, M. Shirakura, E. Nobusawa, M. Tashiro and H. Asanuma, *PLoS One*, 2015, **10**, e0130208.
43 T. K. Sau and C. J. Murphy, *J. Am. Chem. Soc.*, 2004, **126**, 8648–8649.
44 T. K. Sau and C. J. Murphy, *Langmuir*, 2004, **20**, 6414–6420.
45 L. Vigderman, P. Manna and E. R. Zubarev, *Angew. Chem., Int. Ed.*, 2012, **51**, 636–641.
46 Y. Hirabayashi, H. Kurata, H. Funato, T. Nagamine, C. Aizawa, S. ichi Tamura, K. Shimada and T. Kurata, *Vaccine*, 1990, **8**, 243–248.
47 K. Ikeda, A. Ainai and H. Hasegawa, *Vaccine*, 2015, **33**, 6066–6069.
48 Y. Asahi, T. Yoshikawa, I. Watanabe, T. Iwasaki, H. Hasegawa, Y. Sato, S. Shimada, M. Nanno, Y. Matsuoka, M. Ohwaki, Y. Iwakura, Y. Suzuki, C. Aizawa, T. Sata, T. Kurata and S. Tamura, *J. Immunol.*, 2002, **168**, 2930–2938.
49 J. Stevens, A. L. Corper, C. F. Basler, J. K. Taubenberger, P. Palese and I. A. Wilson, *Science*, 2004, **303**, 1866–1870.
50 K. Tobita, A. Sugiura, C. Enomote and M. Furuyama, *Med. Microbiol. Immunol.*, 1975, **162**, 9–14.
51 M. B. Lutz, N. Kukutsch, A. L. Ogilvie, S. Rößner, F. Koch, N. Romani and G. Schuler, *J. Immunol. Methods*, 1999, **223**, 77–92.
52 A. Gole and C. J. Murphy, *Chem. Mater.*, 2004, **16**, 3633–3640.
53 B. B. Aggarwal, *Nat. Rev. Immunol.*, 2003, **3**, 745–756.
54 J. Bradley, *J. Pathol.*, 2008, **214**, 149–160.
55 A. Satie, S. Mazaud-Guittot, I. Seif, D. Mahé, Z. He, G. Jouve, B. Jégou and N. Dejucq-Rainsford, *J. Biol. Chem.*, 2011, **286**, 23280–23295.
56 M. Matsumoto, M. Tatematsu, F. Nishikawa, M. Azuma, N. Ishii, A. Morii-Sakai, H. Shime and T. Seya, *Nat. Commun.*, 2015, **6**, 6280.
57 J. E. Sims and D. E. Smith, *Nat. Rev. Immunol.*, 2010, **10**, 89–102.
58 Z. Ji, X. Wang, H. Zhang, S. Lin, H. Meng, B. Sun, S. George, T. Xia, A. E. Nel and J. I. Zink, *ACS Nano*, 2012, **6**, 5366–5380.
59 B. Sun, Z. Ji, Y. P. Liao, M. Wang, X. Wang, J. Dong, C. H. Chang, R. Li, H. Zhang, A. E. Nel and T. Xia, *ACS Nano*, 2013, **7**, 10834–10849.
60 T. Kusaka, M. Nakayama, K. Nakamura, M. Ishimiya, E. Furusawa and K. Ogasawara, *PLoS One*, 2014, **9**, e92634.